

Medium effects in the production and decay of vector mesons in pion-nucleus reactions*

Ye.S. Golubeva¹, L.A. Kondratyuk² and W. Cassing³

¹ Institute of Nuclear Research, 117312 Moscow, Russia

² Institute of Theoretical and Experimental Physics, 117259 Moscow, Russia

³ Institute for Theoretical Physics, University of Giessen, D-35392 Giessen, Germany

Abstract

The ω -, ρ - and ϕ -resonance production and their dileptonic decay in $\pi^- A$ reactions at 1.1 - 1.7 GeV/c are calculated within the intranuclear cascade (INC) approach. The invariant mass distribution of the dilepton pair for each resonance can be decomposed in two components which correspond to their decay 'inside' the target nucleus and in the vacuum, respectively. The first components are strongly distorted by the nuclear medium due to resonance-nucleon scattering and a possible mass shift at finite baryon density. These medium modifications are compared to background sources in the dilepton spectrum from πN bremsstrahlung as well as the Dalitz decays of ω and η mesons produced in the reaction. Detailed predictions for $\pi^- Pb$ reactions at 1.3 and 1.7 GeV/c are made within several momentum bins for the lepton pair.

PACS: 25.80.-e, 25.80.Hp

Keywords: leptons, pion induced reactions

*Supported by DFG

1 Introduction

The question about the properties of hadronic resonances in the nuclear medium has received a vivid attention during the last years (cf. Refs. [1, 2, 3, 4, 5]). Here, QCD inspired effective Lagrangian models [1, 2, 3] or approaches based on QCD sum rules [4, 5] predict that the masses of the vector mesons ρ , ω and ϕ should decrease with the nuclear density. Furthermore, along with a dropping mass the phase space for the resonance decay also decreases which results in a modification of the resonance width in matter. On the other hand, due to collisional broadening - which depends on the nuclear density and the resonance-nucleon interaction cross section (cf. Refs. [6, 7]) - the resonance width will increase again.

The in-medium properties of vector mesons have been addressed experimentally so far by dilepton measurements at the SPS, both for proton-nucleus and nucleus-nucleus collisions [8, 9, 10, 11]. As proposed by Li *et al.* [12], the enhancement in $S + Au$ reactions compared to $p + Au$ collisions in the invariant mass range $0.3 \leq M \leq 0.7$ GeV might be due to a shift of the ρ meson mass. The microscopic transport studies in Refs. [13, 14, 15] for these systems point in the same direction, however, also more conventional selfenergy effects cannot be ruled out at the present stage [13, 16, 17, 18]. It is therefore necessary to have independent information on the vector meson properties from reactions, where the dynamical picture is more transparent, i.e. in pion-nucleus collisions. Here, especially the ω meson can be produced with low momenta in the laboratory system, such that a substantial fraction of them will also decay inside a heavy nucleus [19, 20]. The same holds for the ϕ meson, however, its vacuum decay will still dominate except for very low momenta in the laboratory.

The mass distributions of the vector mesons in the latter case are expected to have a two component structure [7] in the dilepton invariant mass spectrum: the first component corresponds to resonances decaying in the vacuum, thus showing the free spectral function which is very narrow in case of the ω or ϕ meson; the second (broader) component then corresponds to the resonance decay inside the nucleus. We will use that (in first order) the in-medium resonance can also be described by a Breit-Wigner formula with a mass and width distorted by the nuclear environment.

In this paper we will carry out microscopic calculations for the production and dileptonic decay of ω , ρ and ϕ resonances in $\pi^- A$ collisions at pion momenta of 1.1 - 1.7 GeV/c available at GSI in the near future. The calculations are performed within the framework of the intranuclear cascade model (INC) [21] which was extended earlier [22, 23] to account for the in-medium resonance decays. First calculations for the shapes of the ω and ρ peaks in proton (antiproton) induced reactions $pA \rightarrow VX \rightarrow e^+e^-X$ ($\bar{p}A \rightarrow VX \rightarrow e^+e^-X$) have been reported in Refs. [22, 23]. Here we consider explicitly π^- induced reactions and also compute the background sources in the dilepton spectrum from pion-nucleon bremsstrahlung as well as the Dalitz decays $\omega \rightarrow \pi^0 e^+ e^-$ and $\eta \rightarrow \gamma e^+ e^-$ following Refs. [13, 14, 20, 24].

Our work is organized as follows: In Section 2 we will briefly derive the two-component structure of the resonance decays and provide a description of the intranuclear cascade model (INC) including the resonance cross sections employed. In Section

3 we analyse in detail the production and decay of ω mesons as a function of their laboratory momentum, the nuclear target as well as the initial pion laboratory momentum. Section 4 is devoted to a study of ϕ meson production and decay in $\pi^- Pb$ reactions at 1.7 GeV/c while section 5 concludes our study with a summary and discussion of open problems.

2 Theoretical framework

2.1 The two-component structure of the resonance decay

As it was shown in Ref. [7] the amplitude describing the production of a resonance in a finite nucleus is a superposition of two contributions arising from decays of the resonance 'inside' and 'outside' the nucleus. In Ref. [7] the main emphasis was put on the derivation of the Green function which describes the propagation of the hadronic resonances in the nuclear medium. Whereas the latter work was performed in the framework of multiple scattering theory, here we present an equivalent derivation using the optical potential approach which was applied successfully to the description of pion-nucleus interactions before (cf. [25]).

We start from the relativistic form of the wave equation which describes the propagation of a resonance R in the nuclear medium

$$(-\vec{\nabla}^2 + M_R^2 - iM_R\Gamma_R + U(\vec{r}))\Psi(\vec{r}) = E^2\Psi(\vec{r}), \quad (1)$$

where $E^2 = \vec{p}^2 + M_R^2$; \vec{p} , M_R and Γ_R are the momentum, mass and width of the resonance, respectively. The optical potential then is defined as

$$U(\vec{r}) = -4\pi f(0)\rho_A(\vec{r}) \quad (2)$$

where $f(0)$ is the forward RN -scattering amplitude and ρ_A is the nuclear density.

It is useful to rewrite Eq. (1) in the form

$$(\vec{\nabla}^2 + \vec{p}^2)\Psi(\vec{r}) = (U(\vec{r}) - \Delta)\Psi(\vec{r}), \quad (3)$$

where

$$\Delta = P^2 - M_R^2 - iM_R\Gamma_R \quad (4)$$

is the inverse resonance propagator. The four-momentum P in (4) can be defined through the four-momenta of the resonance decay products,

$$P = p_1 + p_2 + \dots \quad (5)$$

Let us consider the case of a fast resonance, i.e. $pR_A \gg 1$, where R_A is the nuclear radius. In case of a Pb-target this implies $p \gg 30$ MeV/c. For such a case the eikonal approximation can be used and the Green function describing the propagation of the resonance from the point $\vec{r} = (\vec{b}, z)$ to $\vec{r}' = (\vec{b}', z')$ can be written as

$$G_p(\vec{b}', z'; \vec{b}, z) = \frac{1}{2ip} \exp\left\{i \int_z^{z'} \left[p + \frac{1}{2p}(\Delta + 4\pi f(0)\rho_A(\vec{b}, \zeta))\right] d\zeta\right\}$$

$$\times \delta(\vec{b} - \vec{b}')\theta(z' - z), \quad (6)$$

where the z -axis is directed along the resonance momentum \vec{p} , while \vec{b} is the impact parameter.

We will consider here pion energies slightly above threshold, such that the vector mesons ρ, ω and ϕ can be produced only in the first hard pion-nucleon collision. Being produced in the point $\vec{r} = (\vec{b}, z)$ inside the nucleus the vector meson then propagates to the point $\vec{r}' = (\vec{b}', z')$, where it decays into a dilepton pair with the total momentum \vec{P} and invariant mass \vec{P}^2 . The corresponding amplitude can be written as

$$M(\vec{P}, P^2; \vec{b}, z) = N f_{\pi^- N_j \rightarrow R X_i} \int d^2 \vec{b}' dz' \{ \exp(-i\vec{p}\vec{r}') G_p(\vec{r}' - \vec{r}) \exp(i\vec{p}\vec{r}) \} f_{R \rightarrow e^+ e^-}, \quad (7)$$

where $f_{\pi^- N_j \rightarrow R X_i}$ is the production amplitude, $X_i = N, \Delta, \dots$, $f_{R \rightarrow e^+ e^-}$ is the decay amplitude and N a normalization factor which includes also the shadowing effect.

The point $\vec{r}' = (\vec{b}', z')$ of the resonance decay can be inside or outside the nucleus. Accordingly the exponent of the Green function (6) can be separated into the contributions from the two regions

- 1) $z \leq z' \leq z_s = \sqrt{R_A^2 - \vec{b}^2}$ and
- 2) $z' \geq z_s = \sqrt{R_A^2 - \vec{b}^2}$.

When the resonance decays inside the nucleus of radius R_A , only the first part contributes and the inverse resonance propagator has the form

$$\Delta^* = \Delta + 4\pi f(0)\rho_0 = P^2 - M_R^{*2} + iM_R^* \Gamma_R^* \quad (8)$$

where

$$M_R^{*2} = M_R^2 - 4\pi \text{Re}f(0)\rho_A, \quad (9)$$

$$M_R^* \Gamma_R^* = M_R \Gamma_R + 4\pi \text{Im}f(0)\rho_A. \quad (10)$$

If the resonance decays outside the nucleus, both regions contribute and the amplitude for lepton pair production can be written as

$$M_j^i(\vec{P}, P^2; \vec{b}, z) = N f_{\pi^- N_j \rightarrow R X_i} \{ A_{in}(\vec{P}, P^2; \vec{b}, z) + A_{out}(\vec{P}, P^2; \vec{b}, z) \} f_{R \rightarrow e^+ e^-}. \quad (11)$$

In Eq. (11) the contributions from the first and second part can be expressed as

$$A_{in}(\vec{P}, P^2; \vec{b}, z) = \frac{1 - \exp[i(\Delta^*/2k)(z_s - z)]}{\Delta^*}, \quad (12)$$

and

$$A_{out} = \frac{\exp[i(\Delta^*/2k)(z_s - z)]}{\Delta}. \quad (13)$$

Finally, the dilepton invariant mass spectrum is given by the following expression:

$$\frac{d\sigma}{dM} = \sum_{i,j} \int d^2 b dz \rho(\vec{b}, z) |M_j^i(\vec{P}, \vec{P}^2, \vec{b}, z)|^2, \quad (14)$$

where the sum is taken over all nucleons in the target and all production channels, respectively.

When the resonance decays inside the nucleus, its explicit form is described (in a first approximation) by a Breit–Wigner formula

$$F(M) = \frac{1}{2\pi} \frac{\Gamma_R^*}{(M - M_R^*)^2 + \Gamma_R^{*2}/4} \quad (15)$$

that contains the effects of collisional broadening,

$$\Gamma_R^* = \Gamma_R + \delta\Gamma, \quad (16)$$

where

$$\delta\Gamma = \gamma v \sigma_{(RN)} \rho_A, \quad (17)$$

and a shift of the meson mass

$$M_R^* = M_R + \delta M_R, \quad (18)$$

where

$$\delta M_R = -\gamma v \sigma_{(RN)} \rho_A \alpha. \quad (19)$$

In Eqs. (17) and (19) v is the resonance velocity with respect to the target at rest, γ is the associated Lorentz factor, ρ_A is the nuclear density, $\sigma_{(RN)}$ is the resonance–nucleon total cross section and $\alpha = (\text{Re}f(0))/(\text{Im}f(0))$.

If the ratio α is small - which is actually the case for the reactions considered because many reaction channels are open - the broadening of the resonance will be the main effect. The sign of the mass shift depends on the sign of the real part of the forward RN scattering amplitude which, in principle, also depends on the momentum of the resonance. For example, at low energy various authors [1, 2, 4, 5] predict a decreasing mass of the vector mesons ρ , ω and ϕ with the nucleon density, whereas Eletsky and Ioffe have argued recently [26] that the ρ should become heavier in nuclear matter at momenta of 2-7 GeV/c. We will not address this question further since we will concentrate essentially on vector mesons with low momenta relative to the nuclear target and model the mass shift δM_R independently.

2.2 The intranuclear cascade model

In the following we consider the reaction $\pi^- A \rightarrow V X \rightarrow e^+ e^- X$ for different targets at pion momenta from 1.1 up to 1.7 GeV/c. The yields of vector mesons (ω , ρ and ϕ) are calculated within the framework of the intranuclear cascade model (INC) developed in Ref. [21, 27]. In the INC the linearized kinetic equation for the many-body distribution function - describing the hadron transport in nuclear matter [28] - is solved numerically by assuming that during the evolution of the cascade the properties of the target nucleus remain unchanged. This implies that the number of cascade particles N_c is much less than the number of nucleons A_t in the target nucleus, i.e. $N_c \ll A_t$. Since the nucleus is a finite open system with a relatively small number of nucleons, the latter condition

is violated for πN interactions at energies $E_\pi > 3 - 5$ GeV [29] when multiple pion production becomes dominant.

Within the INC approach the target nucleus is regarded as a mixture of degenerate neutron and proton Fermi gases in a spherical potential well of diffuse surface. The momentum distribution of the nucleons is treated in the local density approximation for a Fermi gas. Restricting ourselves to pion momenta below 1.7 GeV/c we have to take into account the following elementary processes:

$$\pi^- p \rightarrow \omega n, \quad (20)$$

$$\pi^- N \rightarrow \omega \pi N \quad (21)$$

$$\pi^- p \rightarrow \rho n, \quad (22)$$

$$\pi^- N \rightarrow \rho \pi N \quad (23)$$

$$\pi^- p \rightarrow \phi n. \quad (24)$$

For the process (20) we use a parametrization of the experimental data from Ref. [27, 30]:

$$\sigma(\pi^- p \rightarrow \omega n) = C \frac{P_{\pi N} - P_\omega^0}{P_{\pi N}^\alpha - d}, \quad (25)$$

where $P_{\pi N}$ is the relative momentum (in GeV/c) of the pion-nucleon pair while $P_\omega^0 = 1.095$ GeV/c is the threshold value. The parameters $C = 13.76$ mb (GeV/c) $^{\alpha-1}$, $\alpha=3.33$ and $d=1.07$ (GeV/c) $^\alpha$ describe satisfactorily the data on the energy-dependent cross section (20) in the near-threshold energy region.

For the inclusive ω production (21) we use the parametrization from Ref. [31]:

$$\sigma(\pi^- p \rightarrow \omega \pi N) = a(x - 1)^b x^{-c}, \quad (26)$$

where the scaling variable is defined as $x = s/s_{th}$; for ω - production we have $s_{th} = 2.958$ GeV 2 , $a = 4.8$ mb, $b = 1.47$, $c = 1.26$. Furthermore, we use

$$\sigma_{\pi^- n \rightarrow \omega \pi N} = 3\sigma_{\pi^- p \rightarrow \omega \pi N} \quad (27)$$

for the isospin dependence in the entrance channel according to a Δ intermediate state.

For ρ^0 -meson production (22), (23) we use the same cross sections as for ω -mesons; this holds experimentally within 20%. Since we will calculate ϕ meson production at a pion momentum of 1.7 GeV/c, only channel (24) contributes to ϕ meson production. In our calculations we use the parametrization of the cross section from Ref. [31] for the exclusive channel, i.e.

$$\sigma_{\pi^- p \rightarrow \phi N}(s) = A \frac{\Gamma^2}{(\sqrt{s} - M_R)^2 + \Gamma^2/4} \frac{\pi^2 |p_\phi|}{4p_\pi^2 s} \quad (28)$$

with $A = 0.00588$ mb GeV 3 , $\Gamma = 0.99$ GeV and $M_R = 1.8$ GeV, where p_π and p_ϕ denote the pion and ϕ momentum in the cms, respectively. The angular distribution for the

products of all reactions (20) - (24) are considered to be isotropic in the pion-nucleon c.m.s. since we operate close to threshold energies.

Vector mesons in this kinematical range are produced only in the first 'hard' interaction. Since the cross sections for their production are small (about 2 mb for ω and ρ and 20 μb for ϕ), we use the weight - function method to calculate the vector meson production and decay in nuclei, i.e. each vector meson carries a weight

$$W_i = \frac{\sigma_{\pi^- N \rightarrow R+X}(\sqrt{s})}{\sigma_{\pi^- N}^{tot}(\sqrt{s})}, \quad (29)$$

where $\sigma_{\pi^- N}^{tot}$ is the total πN cross section at invariant energy \sqrt{s} .

The propagation of vector mesons that are produced in the elementary subprocesses is described in the same manner as in our previous works [21, 27]. Furthermore, the ω -, ρ - and ϕ -mesons may interact with nucleons or decay inside the nucleus into mesons and dileptons. The competition between their decay to mesons and their interaction with a nucleon is determined by the following expression for the mean free path:

$$1/\lambda = 1/\lambda_{dec} + 1/\lambda_{int}, \quad (30)$$

where $\lambda_{int} = (\rho_A \sigma_{(VN)}^{tot})^{-1}$, $\lambda_{dec} = \gamma\beta/(\Gamma_R)$, ρ_A is the nuclear density, $\sigma_{(RN)}^{tot}$ is the total cross section for the meson-nucleon interaction, $\gamma = (1 - \beta^2)^{-1/2}$ is the Lorentz factor, β the particle velocity in units of c , while Γ_R is the vector meson vacuum width.

The "fate" of ω - and ϕ - mesons in the intranuclear cascade is determined by the total cross sections $(\sigma_{\omega N}^{tot})^{-1}$, $(\sigma_{\rho N}^{tot})^{-1}$, $(\sigma_{\phi N}^{tot})^{-1}$ and the partial cross sections for the following interactions with nucleons:

$$\omega N \rightarrow \omega N, \omega N \rightarrow \pi N, \omega N \rightarrow \pi\pi N, \quad (31)$$

$$\rho N \rightarrow \rho N, \rho N \rightarrow \pi N, \rho N \rightarrow \pi\pi N, \quad (32)$$

$$\phi N \rightarrow \phi N, \phi N \rightarrow \pi N, \phi N \rightarrow \pi\pi N. \quad (33)$$

For these reactions no experimental data are directly available and we have to introduce 'plausible' parametrizations. As a model for the ω - and $\phi - N$ cross sections we use for the total cross section

$$\sigma_{\omega N}^{tot}(p_{lab}) = A + \frac{B}{p_{lab}} \quad (34)$$

with $A = 11$ mb and $B = 9$ mb GeV/c; in case of the ϕ meson we adopt $A = 5$ mb and $B = 4.5$ mb GeV/c. The form (34) guarantees that the collisional width $\delta\Gamma_R$ (17) does not diverge, but becomes constant for $p_{lab} \rightarrow 0$. For the elastic ωN cross section we, furthermore, adopt

$$\sigma_{\omega N}^{el}(p_{lab}) = A \frac{1}{1 + ap_{lab}} \quad (35)$$

with $A = 20$ mb and $a = 1$ GeV ^{-1}c . In case of elastic ϕN reactions we use $A = 10$ mb and also $a = 1$ GeV ^{-1}c .

For the ρ -N total and elastic cross sections we adopt the results of Ref. [32], which have been determined from experimental data for the $\pi N \rightarrow \rho N$ exclusive cross section

in a meson-nucleon-resonance model using the experimental branching ratios for the resonances involved [33]. The channels $\omega N \rightarrow \pi N, \rho N \rightarrow \pi N$ are determined via detailed balance from the inverse reactions (26).

In order to explore the observable consequences of vector meson mass shifts at finite nuclear density the in-medium vector meson masses are modelled according to Hatsuda and Lee [4] as

$$M_R^* = M_R(1 - \alpha\rho_A(r)/\rho_0), \quad (36)$$

where $\rho_A(r)$ is the nuclear density at the resonance decay, $\rho_0 = 0.16 fm^{-3}$, and $\alpha = 0.18$ for the ρ and ω while $\alpha = 0.025$ is taken for the ϕ meson as in Ref. [34].

The decay of the resonances to e^+e^- with their actual spectral shape is performed as in Refs. [22, 23]: when the resonance decays into dileptons inside the nucleus its mass is generated according to a Breit–Wigner distribution with average mass M_R^* (36) and $\Gamma_R^* = \Gamma_R + \delta\Gamma_R$ (16), where the collisional broadening and the mass shift are calculated according to the local nuclear density. Its decay to dileptons is recorded as a function of the corresponding invariant mass bin and the local nucleon density ρ_A . If the resonance leaves the nucleus, its spectral function automatically coincides with the free distribution because δM_R and $\delta\Gamma_R$ are zero in this case.

3 Production and decay of ω mesons

Following the suggestion by Schön et al. [19] we start with the reaction $\pi^- + {}^{208}Pb$ at 1.3 GeV/c and present the calculated longitudinal (P_z) and transverse (P_T) momentum distributions of ω mesons in Fig. 1 which decay inside (solid histograms) and outside (dashed histograms) of the Pb-nucleus. Since the ω decays have been recorded as a function of the nucleon density, the 'inside' component is defined as those ω mesons which decay at densities $\rho \geq 0.03 \rho_0$. As one might expect due to kinematical reasons the longitudinal momentum distribution of ω mesons for the 'inside' component is shifted to lower momenta P_z whereas fast ω 's predominantly decay in the vacuum. A similar correlation also holds for the transverse momentum distribution though it is not as pronounced as for the longitudinal momentum distribution. Thus it is clear that in order to study in-medium decays of ω mesons cuts for low P_z and P_T are favorable.

3.1 Dilepton decay of ω mesons

Including the mass shift of the ω 's as well as collisional broadening (as described in Section 2) we show in Fig. 2 the inclusive differential cross section of the e^+e^- pairs from direct ω decays for different cuts in P_z and P_T . In the lowest momentum interval ($P_z \leq 0.25$ GeV, $P_T \leq 0.25$ GeV) one clearly observes a two peak structure corresponding to the in-medium and vacuum decays, respectively. In order to quantify the ratio from both components we have introduced a cut in invariant mass at $M_c = 0.725$ GeV and integrated the dilepton yield below and above M_c . The quantity

$$R = \frac{\int_0^{M_c} dM N_{e^+e^-}(M)}{\int_{M_c}^{\infty} dM N_{e^+e^-}(M)} \quad (37)$$

thus provides a measure for the in-medium ω decay relative to the vacuum decay. Its actual values for the various momentum cuts are given in Fig. 2 and decrease from $R = 1.16$ (for the lowest momentum bin) with increasing total momentum of the dilepton pair to $R=0.21$ (for the highest momentum bin). Thus in case of a large momentum acceptance of the dilepton spectrometer (HADES [35]) one can use different cuts in longitudinal and transverse momentum to explore the in-medium properties of the ω meson as a function of its momentum with respect to the target nucleus at rest, too.

Since in light nuclei the vacuum decay of the ω will dominate, one has to investigate the target mass dependence of the in-medium component, respectively. The results of our calculations at a pion laboratory momentum of 1.3 GeV/c are displayed in Fig. 3 for ^{208}Pb , ^{90}Zr , ^{40}Ca and ^{12}C in the lowest momentum bin ($P_z \leq 0.25$ GeV/c, $P_T \leq 0.25$ GeV/c) for the dilepton pair. The ratio R (37) here decreases from $R = 1.16$ to $R = 0.44$ when going from the heavy (Pb) to the light target (C). In case of ^{12}C no explicit in-medium peak is visible anymore even for the lowest momentum cut; only a low mass tail of the pronounced peak for the vacuum decay appears. This explicit mass dependence can also be exploited experimentally to prove or disprove in-medium modifications of the ω meson by directly comparing dilepton spectra from light and heavy targets (cf. Section 3.3).

A further question is related to the dependence of the in-medium component as a function of the pion laboratory momentum. One expects the ω production cross section to increase with the pion momentum, however, their average momentum distribution will be shifted to higher momenta, too, such that the in-medium decay component might be reduced at higher energy. We have thus performed calculations for $\pi^- + Pb$ collisions for pion momenta of 1.1, 1.3, 1.5, and 1.7 GeV/c, respectively. The results of our computations for $\pi^- + Pb$ reactions are given in Fig. 4 for the lowest momentum bin ($P_z \leq 0.25$ GeV/c, $P_T \leq 0.25$ GeV/c) of the dilepton pair. The ratio R here (within the numerical accuracy) is roughly constant from 1.3 - 1.7 GeV/c while the cross section increases by about 50%. The largest signal $R = 1.44$ we obtain at 1.1 GeV/c, however, here the cross section is already down by about a factor of 2 as compared to a beam momentum of 1.3 GeV/c. Thus our analysis favors laboratory momenta of about 1.3 GeV/c for the study of the in-medium properties of the ω meson, which is in line with the suggestion by Schön et al. [19].

3.2 Variations of the ω in-medium properties

As discussed in Section 2 the properties of the ω meson due to collisional broadening and a mass shift at finite nucleon density are presently not well known. We thus have to explore different medium effects in order to see if the in-medium ω signal will survive. In this respect we first (artificially) increase the elastic ω N cross section (35) by a factor of 2, but keep the ω mass shift fixed by Eq. (36). The respective ω momentum distributions in the laboratory are displayed in Fig. 5 for the enhanced elastic cross section (full histograms) and the expression (35) (dashed histograms). Here the ω momentum distribution for the inside decay is displayed in the upper part of Fig. 5 while the distribution for the vacuum decay component is shown in the lower part of the

figure. We find that a larger elastic cross section leads to a more efficient stopping of the ω mesons in the nuclear target as seen by the shift of the momentum distributions to lower momenta. As a consequence more ω 's decay inside the target with increasing elastic scattering cross section.

This is shown quantitatively in Fig. 6 for the reaction $\pi^- Pb$ at 1.3 GeV/c for the lowest momentum bin ($P_z \leq 0.25$ GeV/c, $P_T \leq 0.25$ GeV/c). With increasing elastic cross section the signal shape in invariant mass (histogram a) versus histogram b)) is not changed very much, however, the inclusive cross section in the lowest momentum bin increases significantly; the ratio $R \approx 1.16$ for both cases is practically the same. Thus by measuring the dileptons from the ω decay at different momentum bins one is able to extract information on the in-medium scattering cross section of ω 's with nucleons as well.

Another problem is related with the actual mass shift of the ω at finite density. In Eq. (36) we have adopted a coefficient of 0.18 as suggested by QCD sumrules [4]. The sumrule studies are performed for ω meson at rest in the nucleus, however, the ω polarization or selfenergy might well be a function of momentum (as suggested by the studies in Refs. [17, 18] in case of the ρ meson) such that the actual mass shift seen in $\pi^- Pb$ reactions might be different. A clear signal is still expected if the ω mass shift is larger than that assumed in Eq. (36); we thus investigate the question if it still can be extracted from dilepton spectra when it reduces to 50%. The numerical results are shown for this case in Fig. 7 (solid histogram) for the reaction $\pi^- + Pb$ at 1.3 GeV/c for the lowest momentum bin ($P_z \leq 0.25$ GeV/c, $P_T \leq 0.25$ GeV/c) in comparison to the result according to Eq. (36) (dashed histogram). With decreasing mass shift of the ω meson its in-medium decay peak shifts closer to the vacuum decay peak, however, with an experimental resolution $\Delta M \leq 10$ MeV it should still be visible in the experimental spectrum at least for the lowest momentum bin.

3.3 Background processes

A first calculation for the background processes at invariant masses above 0.2 GeV for the reaction $\pi^- Pb$ at 1.3 GeV/c has been given in Ref. [20] integrated over all momenta of the dilepton pair. In the latter work it was found that the background for invariant masses above 0.65 GeV dominantly stems from the ρ^0 decay with a small contribution from $\pi^- N$ bremsstrahlung, while the resonance (Δ) Dalitz decays are negligible as well as proton-neutron bremsstrahlung. Here we repeat the studies of Ref. [20] using the same formfactors for the η and ω Dalitz decays as well as for pion-nucleon bremsstrahlung, however, differentiate with respect to momentum bins. The results of our calculations are shown in Fig. 8 for the reaction $\pi^- Pb$ at 1.3 GeV/c for the inclusive dilepton yield integrated over all momenta (l.h.s.) as well as for the lowest momentum bin ($P_z \leq 0.25$ GeV/c, $P_T \leq 0.25$ GeV/c) (r.h.s.). We find the relative background contributions above 0.65 GeV in the low momentum bin to be in the same order of magnitude as for the momentum integrated spectrum, whereas the inclusive cross section drops by about a factor of 15 for the lowest momentum bin.

For experimental purposes we, furthermore, show the results of our calculation

including the background processes discussed above for the reaction $\pi^- {}^{12}\text{C}$ (dashed histograms) and $\pi^- {}^{208}\text{Pb}$ (solid histograms) at 1.3 GeV/c in Fig. 9 integrated over all momenta (l.h.s.) as well as for the lowest momentum bin ($P_z \leq 0.25$ GeV/c, $P_T \leq 0.25$ GeV/c) (r.h.s.), respectively. In order to allow for a direct comparison, both systems have been normalized to the same differential cross section in the ω vacuum decay peaks. The relative enhancement at invariant masses of 0.65 GeV for the Pb-target is quite pronounced for the lowest momentum bin, however, survives also in the momentum integrated spectra (upper part). Thus the in-medium ω meson properties can be extracted experimentally by comparing directly the dilepton yield from light and heavy targets especially for low momentum cuts. We note that the relative dilepton yield at invariant masses $M \leq 0.65$ GeV is smaller for ${}^{12}\text{C}$ as for Pb because we have normalized to the free ω decay peak which is more pronounced for ${}^{12}\text{C}$ since most of the ω -mesons decay in the vacuum here.

4 ϕ meson production and decay

Apart from the ω meson the in-medium properties of the ϕ meson can be studied as well by $\pi^- A$ reactions. Since for pion momenta of 1.3 GeV/c the ϕ cross section is rather low even for Pb-targets, we perform our analysis at a laboratory momentum of 1.7 GeV/c. The distribution of ϕ mesons in longitudinal momentum (P_z) and transverse momentum (P_t) are displayed in Fig. 10 for the 'inside' and 'outside' component, respectively. Due to the longer lifetime of the ϕ mesons (as compared to ω mesons) and lower in-medium scattering cross sections [36], the 'outside' momentum distribution is considerably larger than the 'inside' momentum distribution. The in-medium properties of the ϕ will thus be harder to observe.

In Fig. 11 we show the invariant mass distribution of dilepton pairs from the background processes as well as ω , ρ^0 and ϕ decays including the mass shift (36) for ω and ρ as well as collisional broadening for all mesons, however, discarding a mass shift of the ϕ meson. The momentum integrated mass spectra for $\pi^- \text{Pb}$ at 1.7 GeV/c are shown in the l.h.s. of Fig. 11 whereas a low momentum cut ($P_z \leq 0.25$ GeV/c, $P_T \leq 0.25$ GeV/c) has been applied in the r.h.s. of Fig. 11. The ϕ peak clearly emerges out of the background from the ρ decay even for the integrated spectra, while the ϕ decay is even more pronounced in the low momentum bin. Thus the ϕ meson can clearly be studied experimentally if the mass resolution ΔM is 10 MeV or less.

We now address the question of in-medium effects on the ϕ meson again for the system $\pi^- \text{Pb}$ at 1.7 GeV/c. The results of our calculations are displayed in Fig. 12 for a low momentum cut ($P_z \leq 0.25$ GeV/c, $P_T \leq 0.25$ GeV/c). The full histogram shows the dilepton spectra without a mass shift for ϕ (cf. Fig. 11) while the dashed histogram includes a ϕ mass shift according to (36) with a 2.5% reduction at ρ_0 according to [4] leading to an in-medium peak shifted by about 25 MeV, which is only visible when applying the cut on low momenta; otherwise only a slight asymmetry in the mass spectrum survives.

We note, however, that the lifetime of the ϕ meson at normal nuclear matter density

might be shorter due to in-medium modifications of the kaons and antikaons because for dropping kaon masses the phase space for the ϕ decay to kaon and antikaon in the medium increases [37]. While there are presently no strong indications for a shift of the kaon mass with density [38], some clear evidence for an in-medium mass change of antikaons could be established [39, 40]. The actual calculations of Ref. [40] indicate that the antikaon should drop in mass by about 20% at normal nuclear matter density roughly in line with the Lagrangian approaches of Kaplan and Nelson [41] or Waas, Kaiser and Weise [42]. As a consequence, the 'inside' component of the ϕ decay should be enhanced in such a scenario. We have also performed studies with a modified decay width of the ϕ to $K\bar{K}$ as

$$\Gamma_K^* = \Gamma_K^0 \left\{ \frac{(M_\phi^{*2} - (M_K + M_{\bar{K}}^*)^2)(M_\phi^{*2} - (M_K - M_{\bar{K}}^*)^2)/M_\phi^{*2}}{M_\phi^2 - 4M_K^2} \right\}^{1/2}, \quad (38)$$

where M_ϕ, Γ_K^0 are the bare ϕ mass and decay width to $K\bar{K}$, respectively, and $M_\phi^*(r)$ is the in-medium mass of the ϕ that drops with density according to Eq. (36) with a coefficient of 0.025 while the antikaon mass $M_{\bar{K}}^*$ drops with density with a coefficient ≈ 0.2 [40]. At normal nuclear matter density the decay width of the ϕ to $K\bar{K}$ thus increases from 3.8 MeV to ≈ 8 MeV by roughly a factor of 2 due to the kaonic decay; however, this additional width is smaller than the collisional broadening of $\delta\Gamma_R \approx 15 - 20$ MeV such that this effect will be hard to see experimentally. We thus discard an explicit representation of this limit in Fig. 12 because it almost coincides with the dashed histogram.

5 Summary

In this work we have presented fully microscopic calculations for dilepton production in pion-nucleus reactions within the INC approach and investigated the various contributing channels as well as in-medium modifications of the vector mesons due to collisional broadening or in-medium mass shifts [1, 2, 4, 5]. Our results for π^- Pb at 1.3 GeV/c indicate that the dominant background for invariant masses M above 0.6 GeV arises from π^-N bremsstrahlung which, however, is still small compared to the yield from the direct vector meson decays. A mass shift of the ρ and ω mesons should be seen experimentally by an enhanced yield in the mass regime $0.65 \leq M \leq 0.75$ GeV and a mass shift of the ρ meson especially in a decrease of the dilepton yield for $M \geq 0.85$ GeV because the ρ almost entirely decays inside a Pb-nucleus. The in-medium modifications of the ω mesons are found to be most pronounced for small momentum cuts on the e^+e^- pair in the laboratory ($P_z \leq 0.25$ GeV/c, $P_T \leq 0.25$ GeV/c).

We have, furthermore, addressed the production and decay of ϕ mesons in π^-A reactions. For π^-Pb at 1.7 GeV/c we find a sufficient cross section for ϕ production; its dilepton decay signal is clearly visible above the background from ρ^0 decays. The in-medium mass shift of the ϕ is expected to be much smaller than that of the ρ, ω mesons and the dominant effect expected is a broadening of the ϕ peak due to elastic ϕN collisions and an enhanced kaonic decay width in-medium due to a dropping antikaon

mass [40, 42]. In order to distinguish experimentally the in-medium ϕ peak from the vacuum decay our analysis indicates that sensible cuts on low dilepton momenta in the laboratory as well as an experimental mass resolution $\Delta M \leq 5$ MeV will be necessary.

The authors acknowledge many helpful discussions with K. Borekov, E.L. Bratkovskaya, H. Bokemeyer, A. Iljinov, W. Koenig, V. Metag, W. Schön, A. Sibirtsev and Yu. Simonov throughout this study.

References

- [1] G. Brown and M. Rho, Phys. Rev. Lett. 66 (1991) 2720.
- [2] C.M. Shakin and W.-D. Sun, Phys. Rev. C 49 (1994) 1185.
- [3] F. Klingl and W. Weise, Nucl. Phys. A 606 (1996) 329; F. Klingl, N. Kaiser and W. Weise, hep-ph/9704398.
- [4] T. Hatsuda and S. Lee, Phys. Rev. C 46 (1992) R34.
- [5] M. Asakawa and C.M. Ko, Phys. Rev. C 48 (1993) R526.
- [6] L. A. Kondratyuk, M. Krivoruchenko, N. Bianchi, E. De Sanctis and V. Muccifora, Nucl. Phys. A 579 (1994) 453.
- [7] K.G. Boreskov, J. Koch, L.A. Kondratyuk and M.I. Krivoruchenko, Phys. of Atomic Nuclei 59 (1996) 1908.
- [8] G. Agakichiev et al., Phys. Rev. Lett. 75 (1995) 1272.
- [9] M.A. Mazzoni, Nucl. Phys. A 566 (1994) 95c.
- [10] T. Åkesson et al., Z. Phys. C 68 (1995) 47.
- [11] A. Drees, Nucl. Phys. A610 (1996) 536c.
- [12] G.Q. Li, C.M. Ko, and G.E. Brown, Phys. Rev. Lett. 75 (1995) 4007.
- [13] W. Cassing, W. Ehehalt and C.M. Ko, Phys. Lett B 363 (1995) 35.
- [14] W. Cassing, W. Ehehalt and I. Kralik, Phys. Lett B 377 (1996) 5.
- [15] E. L. Bratkovskaya and W. Cassing, Nucl. Phys. A 619 (1997) 413.
- [16] R. Rapp, G. Chanfray, and J. Wambach, Phys. Rev. Lett. 76 (1996) 368.
- [17] R. Rapp, G. Chanfray, and J. Wambach, Nucl. Phys. A 617 (1997) 472.
- [18] B. Friman and H.J. Pirner, Nucl. Phys. A 617 (1997) 496.
- [19] W. Schön, H. Bokemeyer, W. Koenig, and V. Metag, Acta Physica Polonica B27 (1996) 2959.
- [20] W. Cassing, Ye.S. Golubeva, A.S. Iljinov, and L.A. Kondratyuk, Phys. Lett. B396 (1997) 26.
- [21] Ye.S. Golubeva, A.S. Iljinov, B.V. Krippa and I.A. Pshenichnov, Nucl. Phys. A 537 (1992) 393.

- [22] Ye.S. Golubeva, A.S. Iljinov and L.A. Kondratyuk, Phys. of Atomic Nuclei 59 (1996) 1894.
- [23] Ye.S. Golubeva, A.S. Iljinov and L.A. Kondratyuk, Acta Physica Polonica B 27 (1996) 3241.
- [24] Gy. Wolf, G. Batko, W. Cassing et al., Nucl. Phys. A 517 (1990) 615;
Gy. Wolf, W. Cassing and U. Mosel, Nucl. Phys. A 552 (1993) 549.
- [25] T. Ericson and W. Weise, *Pions in Nuclei*, Clarendon Press, Oxford 1988.
- [26] V. Eletsky and B.L. Ioffe, Phys. Rev. Lett. 78 (1997) 1010.
- [27] Ye.S. Golubeva, A.S. Iljinov and I.A. Pshenichnov, Nucl. Phys. A 562 (1993) 389
- [28] V.E. Bunakov, Particles and Nuclei (USSR) 11 (1980) 1285.
- [29] V.S. Barashenkov, A.S. Iljinov, N.M. Sobolevsky, and V.D. Toneev, Usp. Fiz. Nauk. 109 (1973) 91.
- [30] J. Cugnon, P. Deneve and J. Vandermeulen, Phys. Rev. C41 (1990) 1339.
- [31] A. Sibirtsev, Nucl. Phys. A604 (1996) 455;
A. Sibirtsev, W. Cassing and U. Mosel, nucl-th/9607047, Z. Phys. A, in print.
- [32] A. Sibirtsev and W. Cassing, preprint UGI-97-08.
- [33] Review of Particle Properties, Phys. Rev. D 50 (1995)
- [34] W. Ehehalt and W. Cassing, Nucl. Phys. A 602 (1996) 449.
- [35] HADES-Collaboration, Proposal for a High-Acceptance Di-Electron Spectrometer, GSI 1994.
- [36] W. S. Chung, G. Q. Li and C. M. Ko, nucl-th/9611024.
- [37] G. Q. Li and C.M. Ko, Nucl. Phys. A 582 (1995) 731.
- [38] E.L. Bratkovskaya, W. Cassing, and U. Mosel, nucl-th/9703047, Nucl. Phys. A, in print.
- [39] G.Q. Li, C.M. Ko and X.S. Fang, Phys. Lett. B 329 (1994) 149.
- [40] W. Cassing, E.L. Bratkovskaya, U. Mosel, S. Teis, and A. Sibirtsev, Nucl. Phys. A 614 (1997) 415.
- [41] D. B. Kaplan and A. E. Nelson, Phys. Lett. B 175 (1986) 57.
- [42] T. Waas, N. Kaiser and W. Weise, Phys. Lett. B 379 (1996) 34.

Figure captions

Fig. 1: The momentum distribution of the ω mesons produced in the reaction $\pi^- + Pb \rightarrow \omega X$ at 1.3 GeV/c as a function of the longitudinal momentum in the laboratory P_z (upper part) and the transverse momentum P_T (lower part); solid histograms: ω mesons decaying inside the nucleus, dashed histograms: ω mesons decaying in the vacuum.

Fig. 2: The inclusive differential cross section of e^+e^- pairs from direct ω decays for $\pi^- + Pb$ at 1.3 GeV/c for different cuts in longitudinal (P_z) and transverse (P_T) momentum. The ratio R (37) provides a measure for the relative weight of the in-component relative to the vacuum component using a cut in invariant mass at $M_c = 0.725$ GeV.

Fig. 3: The inclusive differential cross section of e^+e^- pairs from direct ω decays for π^- induced reactions at 1.3 GeV/c on ^{208}Pb ,⁹⁰ Zr ,⁴⁰ Ca and ^{12}C for a low momentum cut ($P_z \leq 0.25$ GeV/c, $P_T \leq 0.25$ GeV/c). The ratio R (37) provides a measure for the relative weight of the in-component relative to the vacuum component using a cut in invariant mass at $M_c = 0.725$ GeV.

Fig. 4: The inclusive differential cross section of e^+e^- pairs from direct ω decays for π^- induced reactions on ^{208}Pb at 1.1, 1.3, 1.5 and 1.7 GeV/c for a low momentum cut ($P_z \leq 0.25$ GeV/c, $P_T \leq 0.25$ GeV/c). The ratio R (37) provides a measure for the relative weight of the in-component relative to the vacuum component using a cut in invariant mass at $M_c = 0.725$ GeV.

Fig. 5: The momentum distribution of the ω mesons produced in the reaction $\pi^- Pb \rightarrow \omega X$ at 1.3 GeV/c as a function of the momentum in the laboratory P for the 'inside' (upper part) and the 'outside' component (lower part). The dashed histograms result from a calculation using the elastic ωN cross section (35) (b), while the solid histograms reflect a calculation with twice the elastic ωN cross section (a).

Fig. 6: The inclusive differential cross section of e^+e^- pairs from direct ω decays for π^- induced reactions on ^{208}Pb at 1.3 GeV/c for a low momentum cut ($P_z \leq 0.25$ GeV/c, $P_T \leq 0.25$ GeV/c). The dashed histogram (b) results from a calculation using the elastic ωN cross section (35), while the solid histogram (a) reflects a calculation with twice the elastic ωN cross section.

Fig. 7: The inclusive differential cross section of e^+e^- pairs from direct ω decays for π^- induced reactions on ^{208}Pb at 1.3 GeV/c for a low momentum cut ($P_z \leq 0.25$ GeV/c, $P_T \leq 0.25$ GeV/c). The dashed histogram (b) results from a calculation using a ω mass shift of 18% at ρ_0 in (36), while the solid histogram (a) reflects a calculation with half the mass shift (9%).

Fig. 8: The inclusive differential cross section of e^+e^- pairs from π^- induced reactions on ^{208}Pb at 1.3 GeV/c; l.h.s.: integrated over all dilepton momenta; r.h.s.: for a low momentum cut ($P_z \leq 0.25$ GeV/c, $P_T \leq 0.25$ GeV/c). The upper solid line represents the sum of all contributions; the thin histograms present the yields from pion-nucleon bremsstrahlung (πN), the η Dalitz decay (η), the ω Dalitz decay and the direct decays of the vector mesons ρ and ω , respectively.

Fig. 9: Comparison of the inclusive differential cross section of e^+e^- pairs from π^- induced reactions on ^{208}Pb (solid histograms) and ^{12}C (dashed histograms) at 1.3 GeV/c including all sources; l.h.s.: integrated over all dilepton momenta; r.h.s.: for a low momentum cut ($P_z \leq 0.25$ GeV/c, $P_T \leq 0.25$ GeV/c). Both systems have been normalized to the same differential cross section in the ω vacuum decay peaks.

Fig. 10: The momentum distribution of the ϕ mesons produced in the reaction $\pi^- Pb \rightarrow \phi X$ at 1.7 GeV/c as a function of the longitudinal momentum in the laboratory P_z (upper part) and the transverse momentum (P_t) (lower part) for the 'inside' (solid histograms) and the 'outside' components (dashed histograms).

Fig. 11: The invariant mass distribution of dilepton pairs from ω , ρ^0 and ϕ decays for $\pi^- Pb$ at 1.7 GeV/c including the mass shift (36) for ω 's and ρ 's as well as collisional broadening for all mesons, however, discarding a mass shift of the ϕ meson; l.h.s.: momentum integrated mass spectra; r.h.s.: for a low momentum cut ($P_z \leq 0.25$ GeV/c, $P_T \leq 0.25$ GeV/c).

Fig. 12: The invariant mass distribution of dilepton pairs from ω , ρ^0 and ϕ decays for $\pi^- Pb$ at 1.7 GeV/c including the mass shift (36) for ω 's and ρ 's as well as collisional broadening for these mesons for a low momentum cut ($P_z \leq 0.25$ GeV/c, $P_T \leq 0.25$ GeV/c). The full histogram at ≈ 1.02 GeV of invariant mass shows the ϕ decay without a mass shift but collisional broadening (cf. Fig. 11) while the dashed histogram additionally includes a ϕ mass shift according to (36) by 2.5% at ρ_0 .

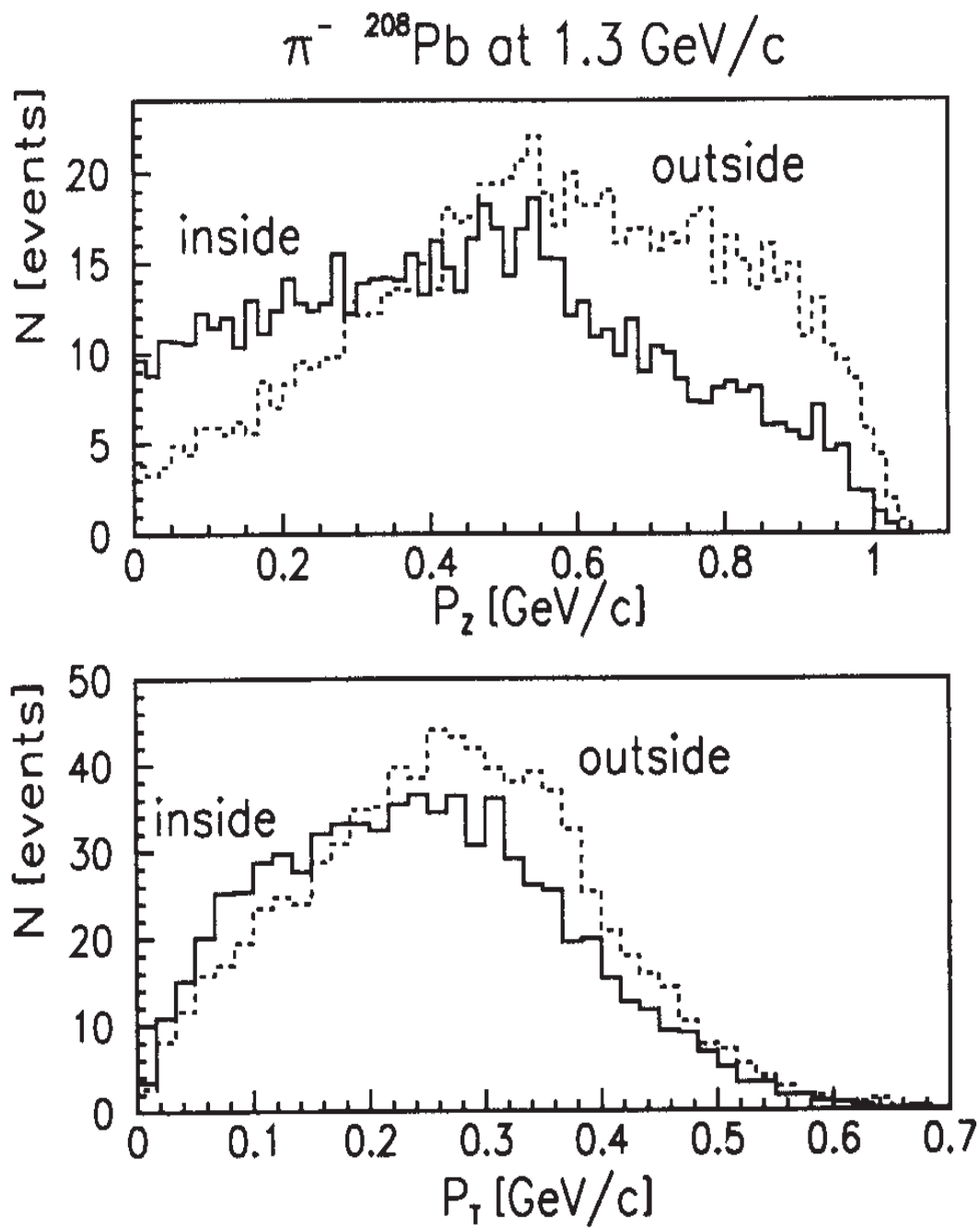


Fig. 1

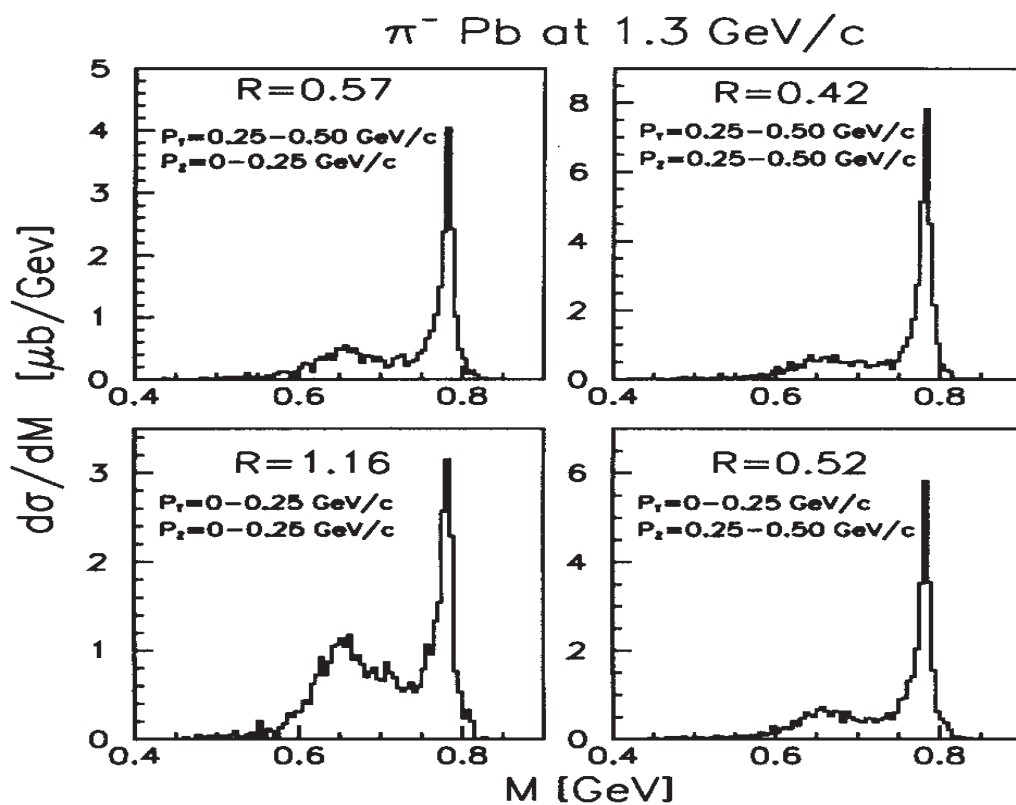
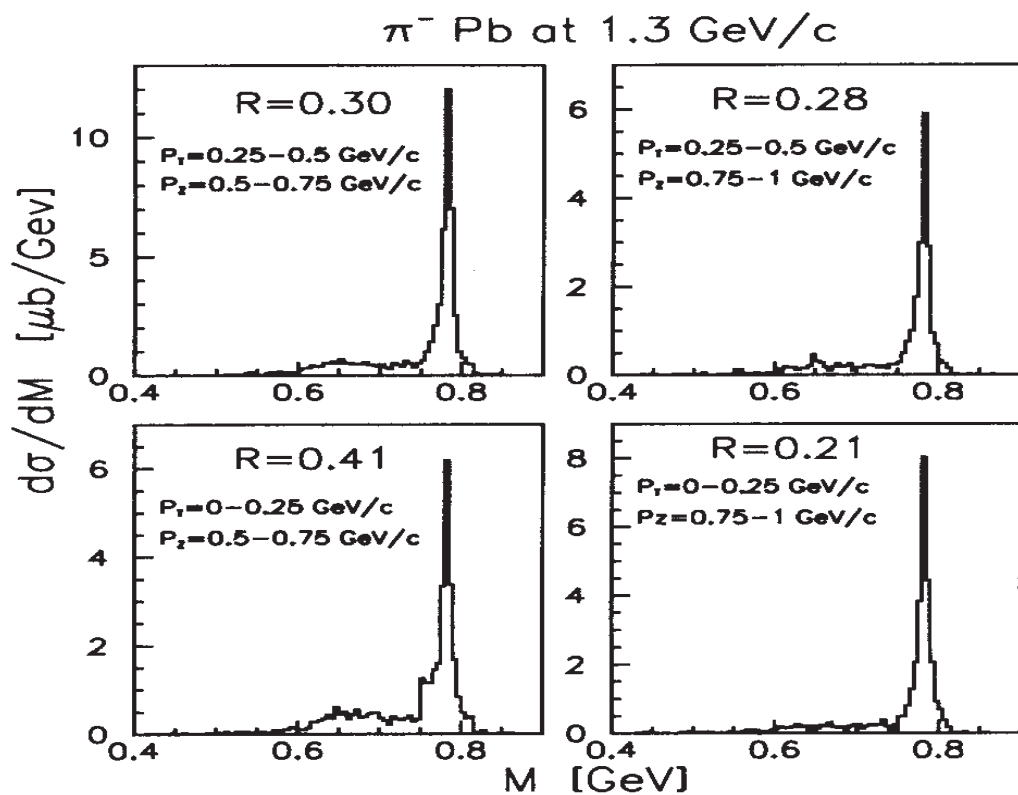


Fig. 2

$\pi^- A$ at 1.3 GeV/c

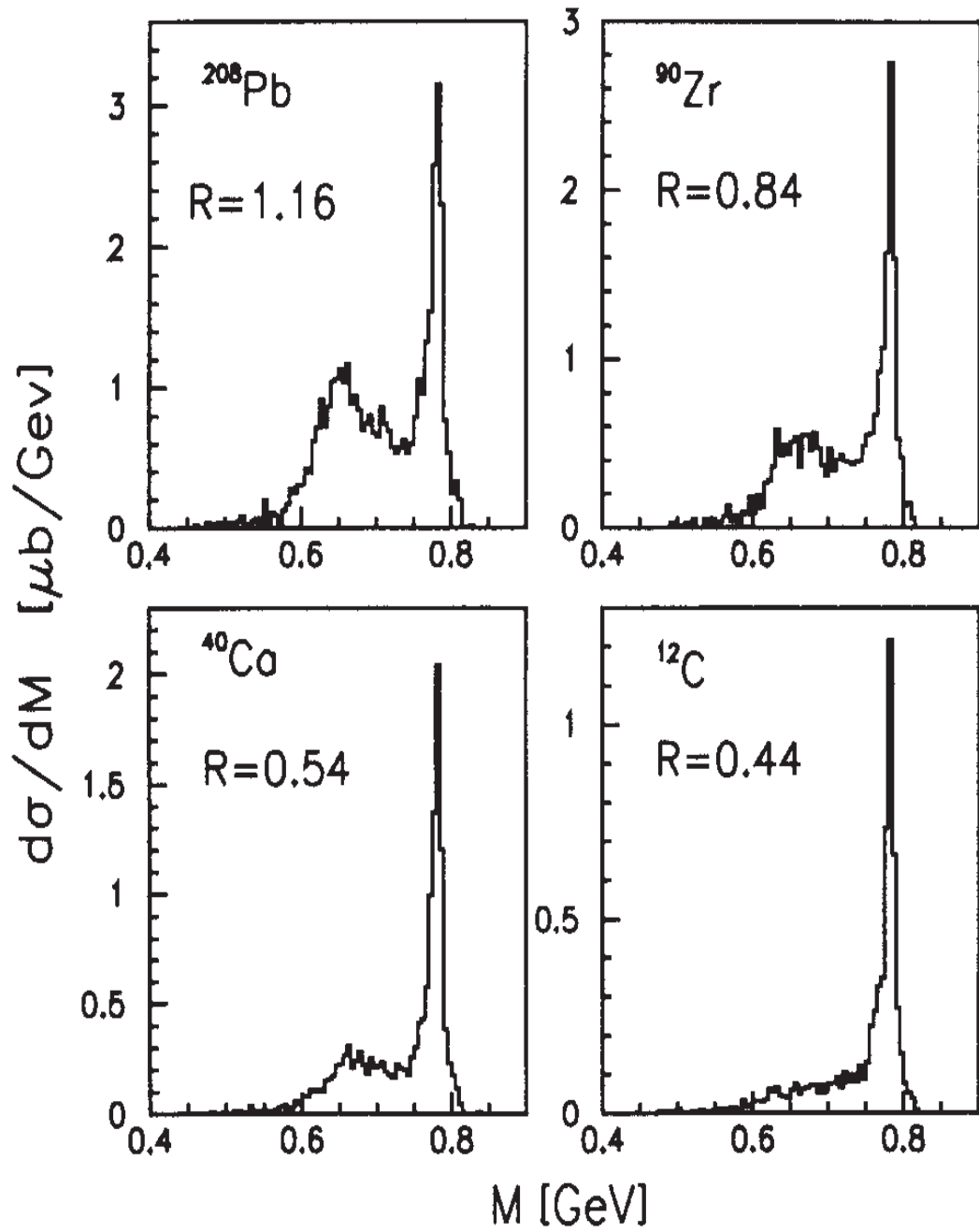


Fig. 3

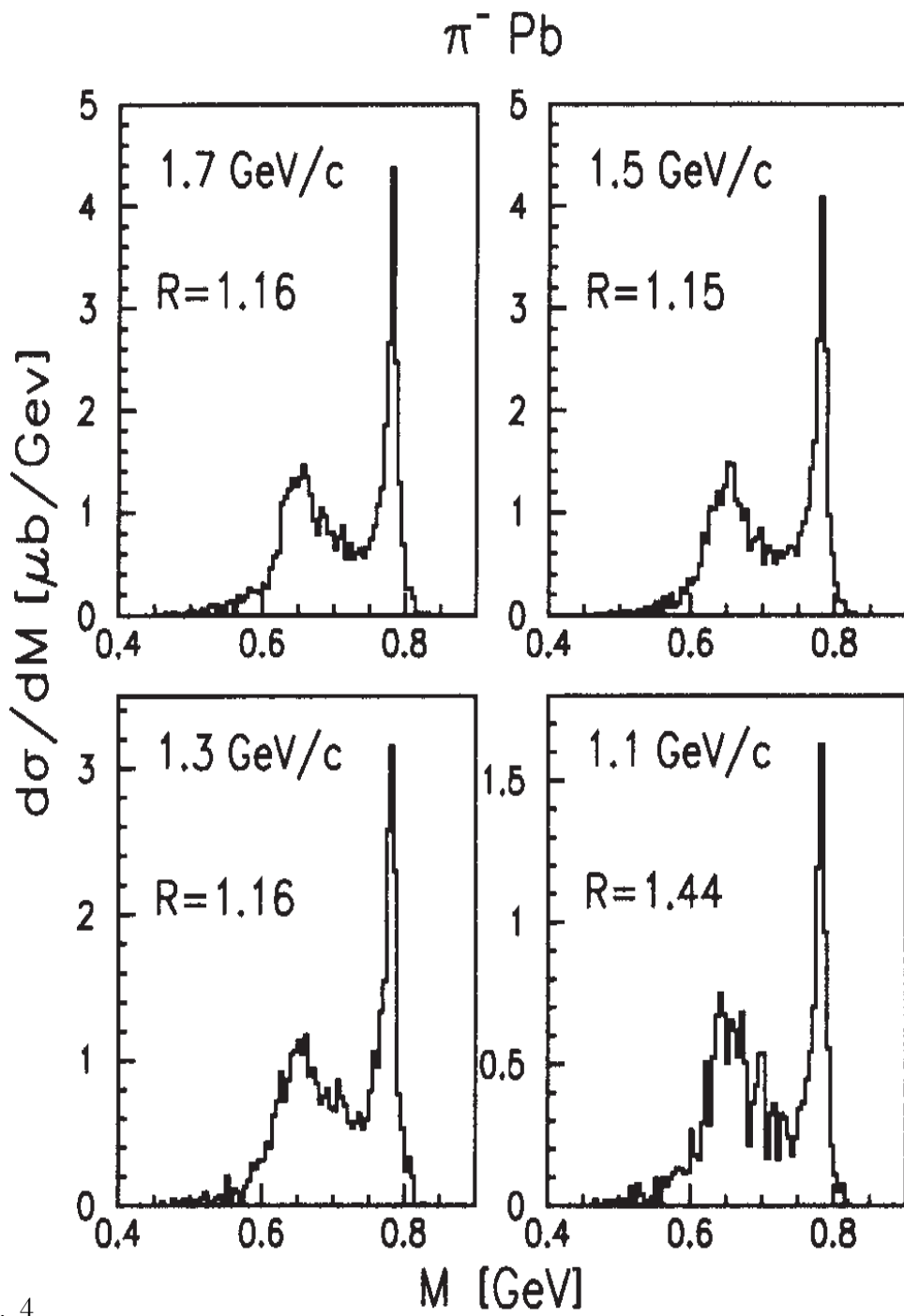


Fig. 4

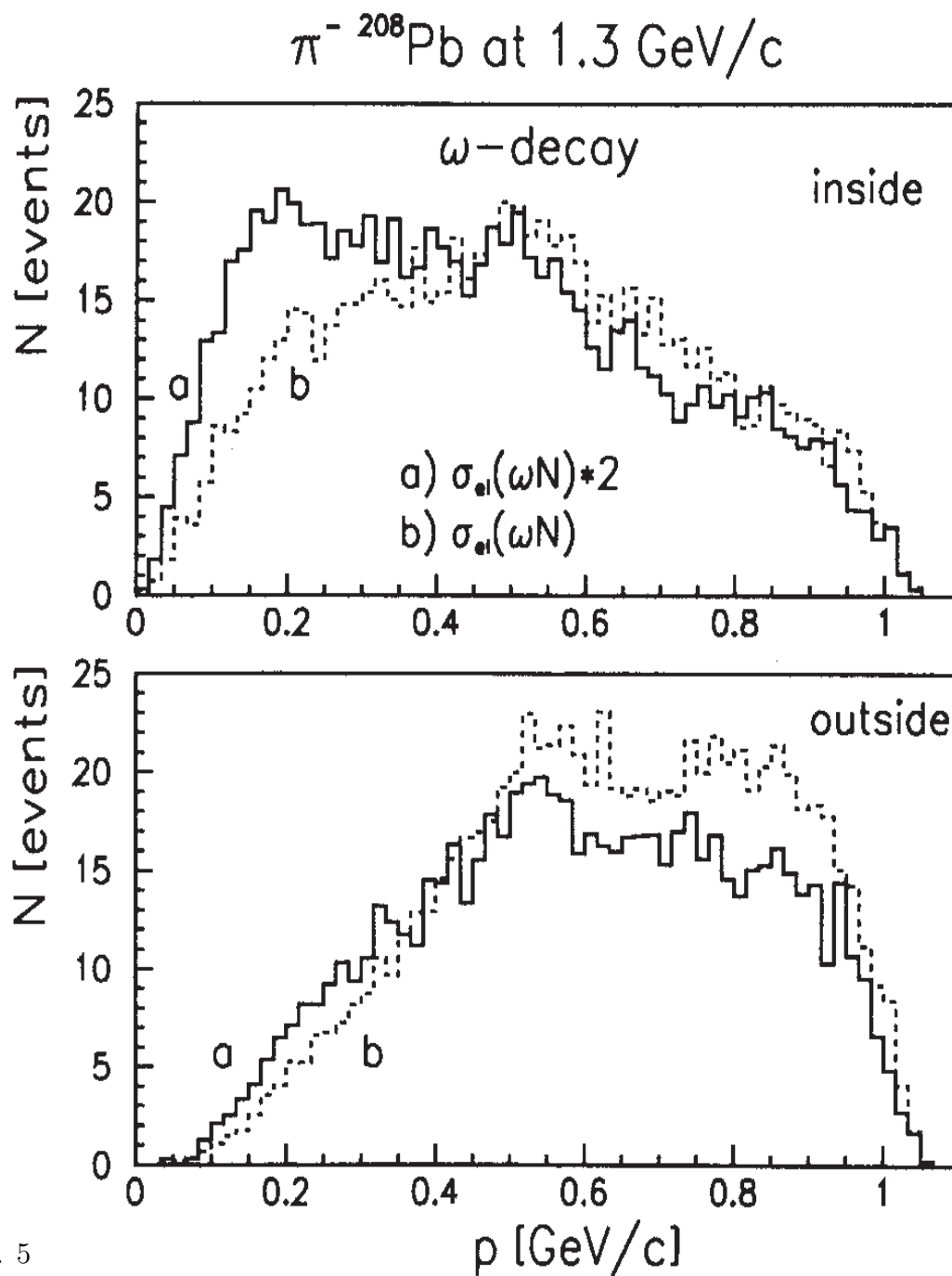


Fig. 5

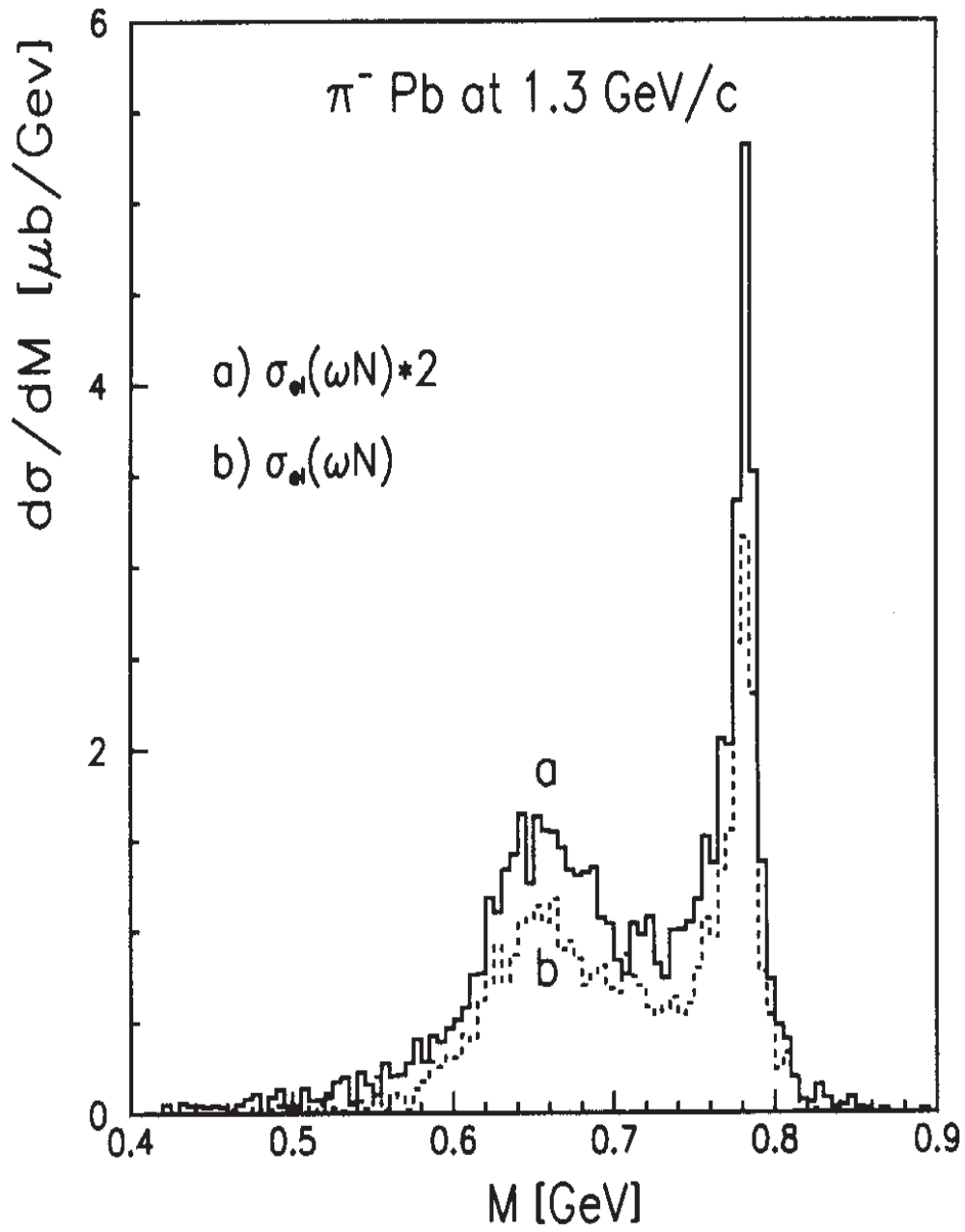


Fig. 6

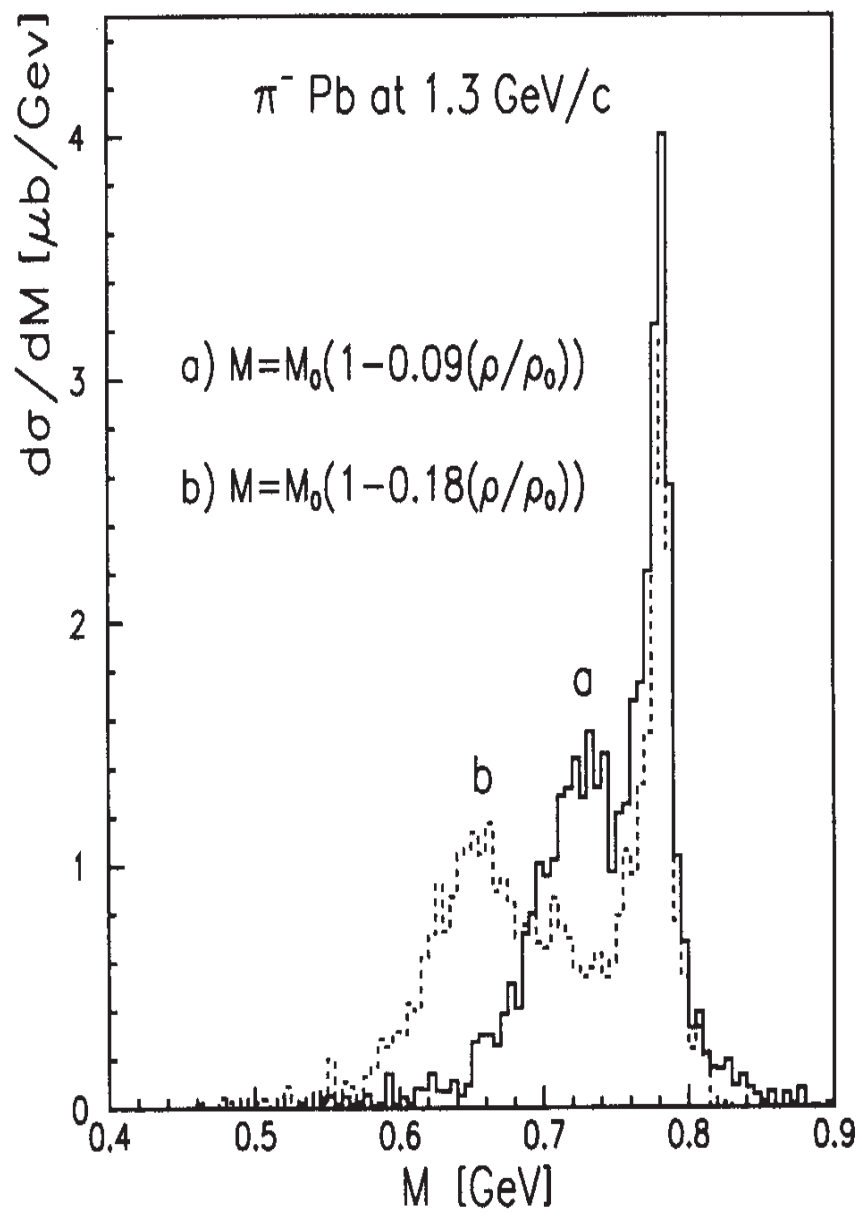


Fig. 7

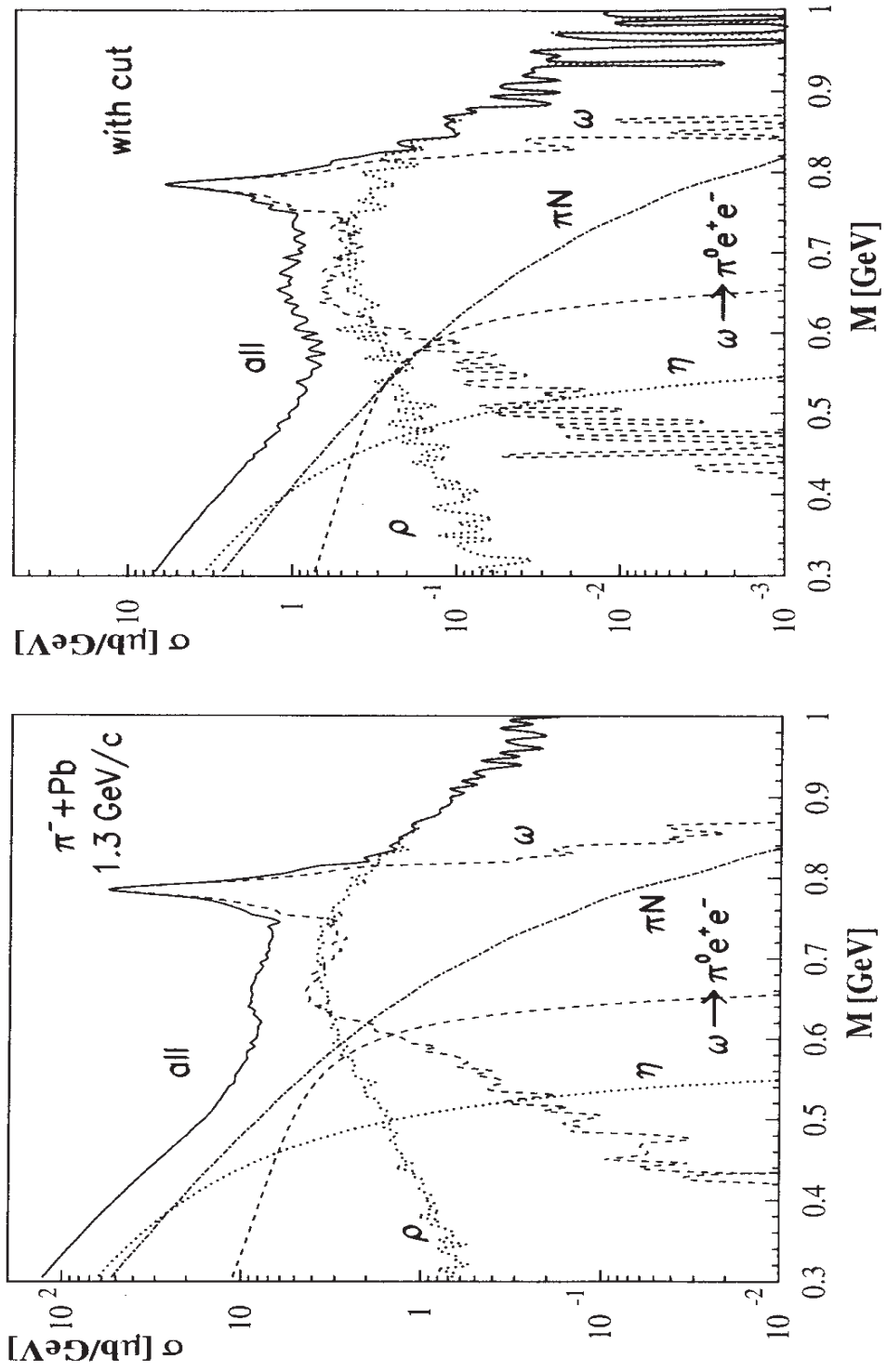


Fig. 8

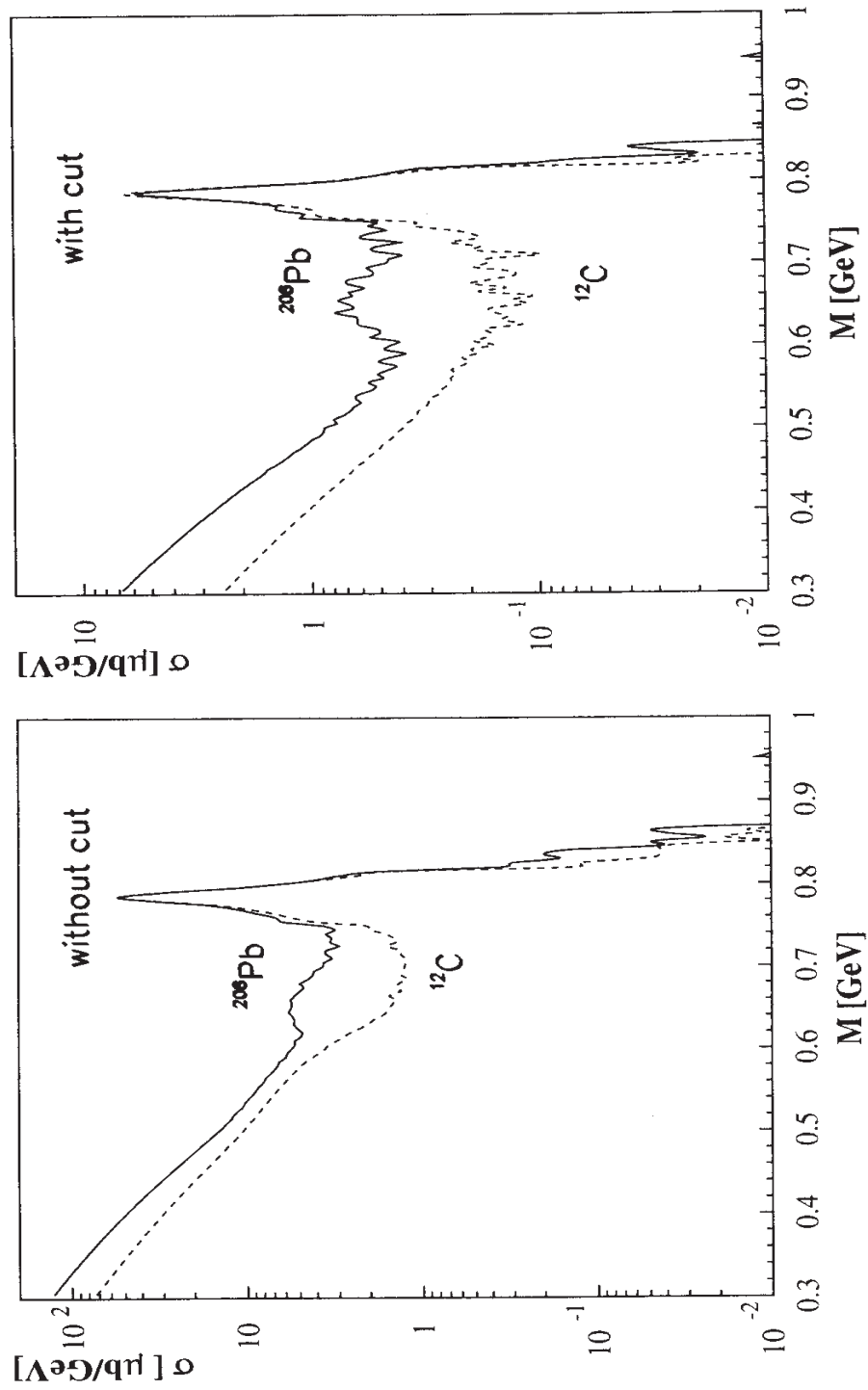


Fig. 9

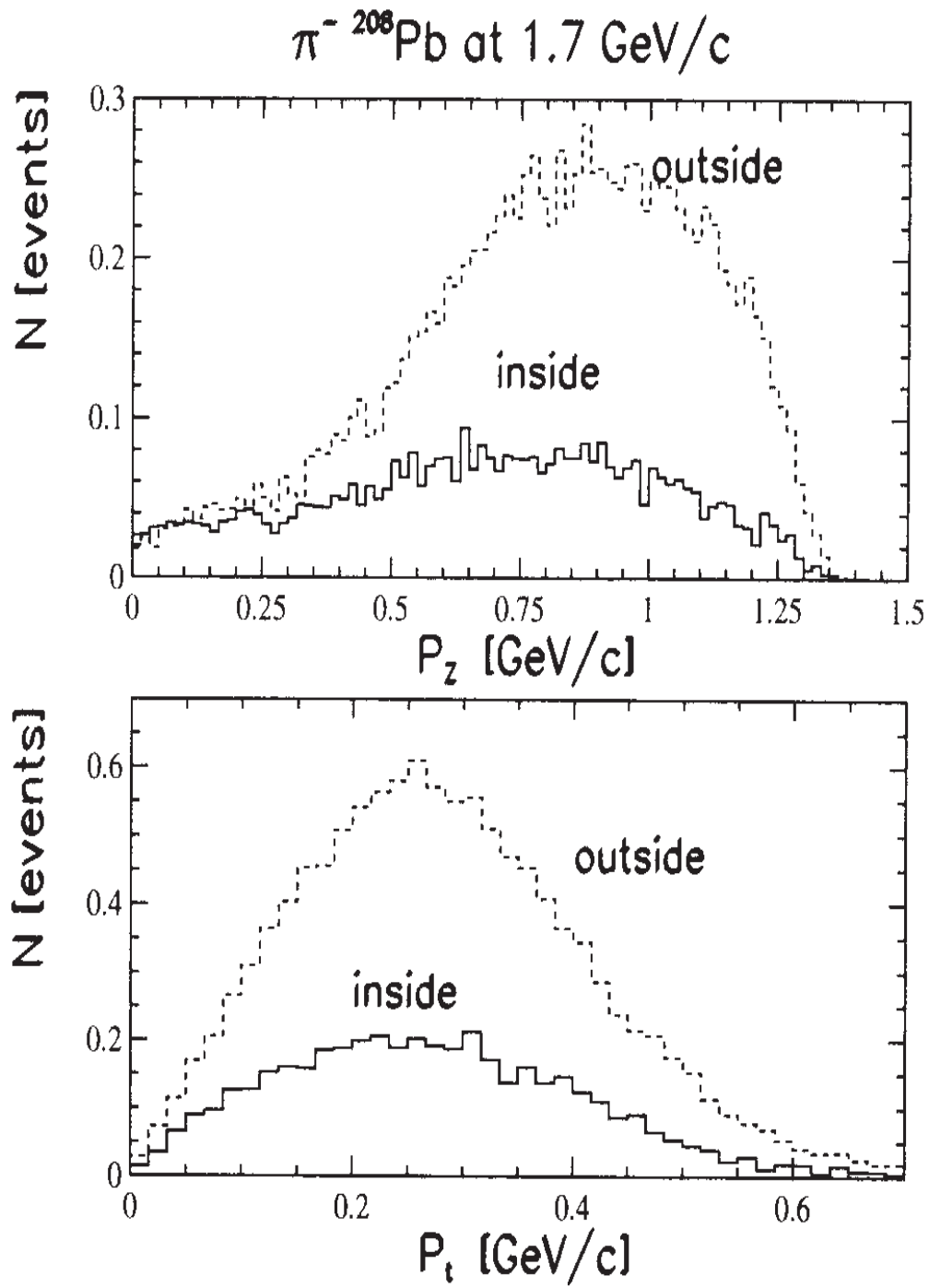


Fig. 10

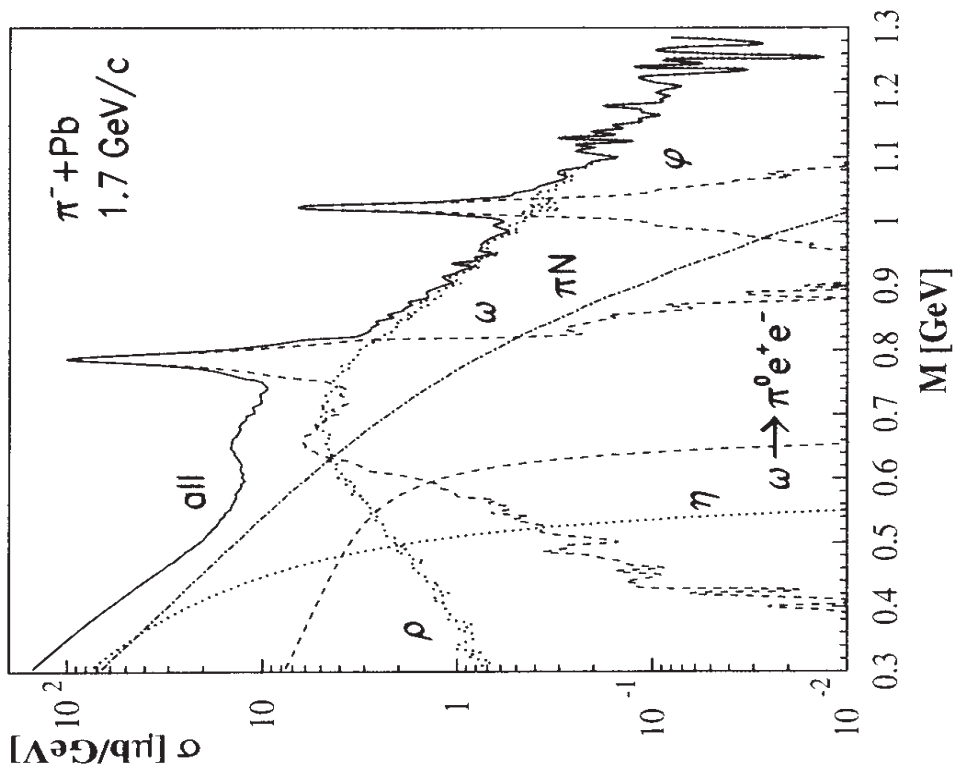
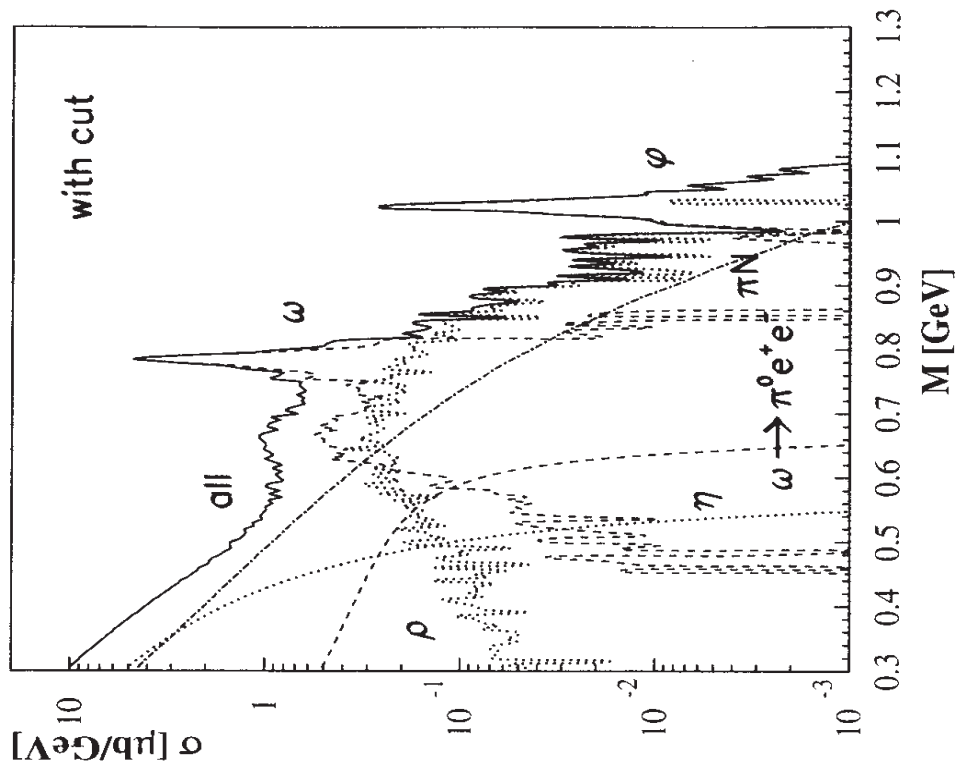


Fig.11

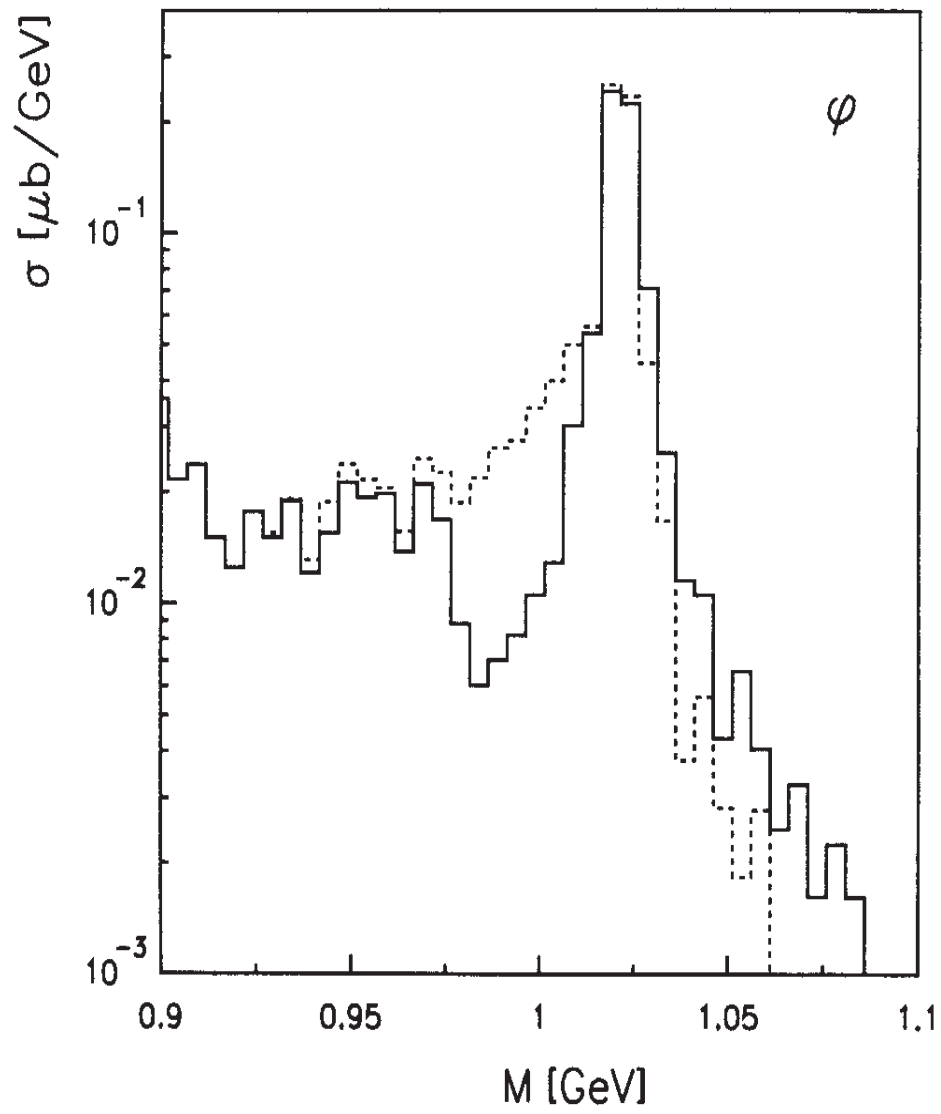


Fig.12